Int J Adv Manuf Technol (2008) 37:747–759
DOI 10.1007/s00170-007-1006-z

ORIGINAL ARTICLE

High-speed contouring enhanced with P-H curves

Behnam Moetakef Imani · Javad Jahanpour

Received: 2 January 2007 / Accepted: 7 March 2007 / Published online: 24 April 2007

Abstract In this paper, Pythagorean hodograph (P-H) curve theory is used for high-speed contouring applications. There are large contouring errors around sharp corners when low-bandwidth servo controllers (such as P-PI control) are used. It is possible to construct a P-H curve in the region of sharp corners in order to decrease the amount of cornering error. The developed algorithm is implemented for various corners with different angles. With respect to sharp tool paths, the total machining time is increased by a small amount, but the cornering error is reduced to the allowable tolerance limit. The results of simulation, such as the total cornering time and the cornering error, are compared with previously published methods. It has been shown that the over-corner P-H approach will substantially decrease the amount of cornering error.

Keywords Numerical control · Real-time interpolation · P-H curves · Cornering error

1 Introduction

The total machining time and maintaining tool path accuracy are among the most important objectives of high-speed machining. When machining sharp corners or tool paths with large variations, there are either sudden changes of direction on axis movements or a sudden stop of motion, which result in large cornering errors. The amount of this error depends on the parameters of the servo axes. In high-speed milling, the selection of the feed rate, acceleration, and deceleration of each axis are extremely important in order to reach a uniform motion [1].

One method of reducing the tracking error of a sharp corner is to substitute a sharp corner with a smooth curve. Jouaneh et al. [2–4] introduced a circular arc and double clothoid curves in the vicinity of corners to obtain a smooth tracking motion in robotic applications. Later, Kanayama and Miyake [5] substituted sharp corners with double clothoid curves in order to smooth the motion transition when tracking corners for a mobile robot. In the following research, Erkorkmaz et al. [6] replaced the line segments of the corner area with two- and three-segment quintic splines. They implemented their algorithm for 30°, 60°, and 90° corners, with constraint of 30 μm for the cornering error. They introduce over-corner and under-corner methods for a P-PI servo controller and a sliding mode controller, respectively. They also compare the simulation results with real experimental results. The nearly arc-length parameterization has been used for the interpolation of a tool path with constant feed rate. The required arc length must be computed by numerical quadrature [7]. Thus, it is not possible to evaluate the exact arc length for the spline curve, which makes interpolation inherently a rough approximation (even at fixed feed rates) [8].

Pythagorean hodograph (P-H) curves were established by Farouki and Sakkalis [9] in 1990. These curves are a special family of freeform curves and a subset of the Bezier representation that are suitable for real-time interpolation at constant or variable feed rates. In contrast with nearly arc-length parameterization, the arc length of P-H curves can be computed precisely by evaluating a

B. M. Imani (✉) · J. Jahanpour
Department of Mechanical Engineering, Engineering Faculty,
Ferdowsi University of Mashad,
Mashad, Iran
e-mail: imani@ferdowsi.um.ac.ir

J. Jahanpour
e-mail: ja_ja27@stu-mail.um.ac.ir

polynomial function of the curve parameter (there is no need for approximate numerical quadrature) [7, 10]. In addition, efforts have been made for spline interpolation in order to reach near-arc-length parameterization. But, if the ratio of the parameter range to the segment arc length differs by as small as 5% between consecutive segments, this will cause a discontinuity in the feed rate profile where spline segments connect [6]. In order to avoid such problems, an iterative interpolation technique has been devised by Erkorkmaz and Altintas [11]. In their method, the parameter related to the desired arc length is computed with limited accuracy. By contrast, for the proposed P-H curve approach, one arc-length parametric curve is defined for the whole corner. Thus, there is no feed rate fluctuation along the actual tool path. Also, the complexity of the P-H curve interpolation is much lower compared to the interpolation of multi-segment quintic splines. Moreover, P-H quintic curves are suitable in practical applications where flexibility is required [12].

At each instant, the geometric deviation between the reference tool path and the actual position of the tool is computed using the method proposed by Erkorkmaz et al. [6, 13]. This technique is used for finding the shortest orthogonal distance between the reference tool path and the actual tool position. The error can be evaluated in the various regions of each corner.

In this paper, a P-H quintic curve is proposed in order to decrease the amount of cornering error. As opposed to a previously proposed method [6] which defines three-segment quintic splines, our method introduces one arc-length parametric P-H curve for the whole corner. The over-corner P-H approach is implemented for a P-PI servo controller.

Henceforth, the paper is organized as follows. In Sect. 2, formulation of the P-H quintic is presented. In Sect. 3, real-time interpolation using the P-H curve approach is introduced. The dynamic model of feed drives and the developed over-corner P-H approach are presented in Sects. 4 and 5, respectively. The simulation results are discussed and compared with previous research work in Sect. 6. Finally, Sect. 7 presents the conclusions of the paper.

2 Pythagorean hodograph quintic curves

In this section, P-H quintic Hermite interpolants are briefly reviewed. In addition, the effect of end-derivative magnitudes on the P-H curve is presented.

2.1 P-H quintic Hermite interpolants

The complex representation for a planar P-H curve is presented by $r(\xi) = x(\xi) + iy(\xi)$, where $\xi \in [0,\ 1]$ is a real parameter [7]. $r(\xi)$ is a P-H curve if there exist polynomials $u(\xi)$, $v(\xi)$ such that its derivative or hodograph, $r'(\xi) = w^2(\xi)$ satisfies:

$$\begin{aligned} &x'(\xi) = u^2(\xi) - v^2(\xi)\,, y'(\xi) = 2u(\xi)v(\xi), \\ &\sigma(\xi) = u^2(\xi) + v^2(\xi) \end{aligned} \tag{1}$$

where $\sigma(\xi) = \sqrt{x'^2(\xi) + y'^2(\xi)}$ is the parametric speed of $r(\xi)$ and the greatest common divisor (GCD) of u and v is equal to 1. The parametric speed of $r(\xi)$ is the rate of arc length variation with respect to parameter ξ, i.e.:

$$\sigma(\xi) = \frac{\mathrm{d}s}{\mathrm{d}\xi} \tag{2}$$

Thus, the integration of σ provides the polynomial cumulative arc length function:

$$s(\xi) = \int_0^{\xi} \sigma(\xi)\mathrm{d}\xi \tag{3}$$

For a P-H quintic, the polynomial $w(\xi) = u(\xi) + iv(\xi)$ must be quadratic. Expressing in Bernstein form, the hodograph is:

$$r'(\xi) = \left[w_0(1-\xi)^2 + w_1 2(1-\xi)\xi + w_2\xi^2\right]^2 \tag{4}$$

Considering the following interpolation conditions:

$$\begin{aligned} &r'(0) = d_0, r'(1) \ = d_1, \\ &\int_0^1 r'(\xi)\mathrm{d}\xi = r_1 - r_0 \end{aligned}$$

where r_0, r_1 are end-points and d_0, d_1 are the corresponding end-derivatives, the coefficients w_0, w_1, and w_2 are solutions to the following system of equations:

$$\begin{aligned} &w_0^2 = d_0,\ w_2^2 = d_1 \\ &\int_0^1 \left[w_0(1-\xi)^2 + w_1 2(1-\xi)\xi + w_2\xi^2\right]^2 \mathrm{d}\xi = r_1 - r_0 \end{aligned} \tag{5}$$

The P-H quintic curves which interpolate the given end-points and end-derivatives are obtained by the following coefficients:

$$\begin{aligned} &w_0 = \pm\sqrt{d_0}\,, \\ &w_2 = \pm\sqrt{d_1} \\ &w_1 = \frac{-3(w_0+w_2) \pm \sqrt{120(r_1-r_0) - 15w_0^2 - 15w_2^2 + 10w_0w_2}}{4} \end{aligned} \tag{6}$$

Considering the signs of w_0, w_1, and w_2, there are four independent P-H quintic interpolants. Moon et al. [7] have recommended the absolute rotation index to select the

acceptable shape. For example, the four P-H quintic curves corresponding to Hermite data, $r_0 = 3 + i$, $r_1 = 5 + i$, $d_0 = 3 - 10i$, and $d_1 = 2 + 8i$ are shown in Fig. 1. It has been observed that the signs (++) for w_0 and w_2 have a smaller absolute rotation index (Rabs), thus, it is the acceptable interpolant.

2.2 Effect of end-derivative magnitude coefficients on the P-H curve shape

In order to show the effect of the end-derivative magnitudes on the P-H curve shape, the following example is presented. First, a P-H curve is interpolated by the following end-points and end-derivatives:

$$r_0 = 0,\ r_1 = 0.5,\ d_0 = 1 + i,\ d_1 = 1 - i$$

The positions of the end-points are kept constant, while the magnitudes of the end-derivatives are changed by multiplying coefficients b_1 and b_2 as follows:

$$d_0' = b_1 d_0 = b_1(1 + i), \qquad (7)$$
$$d_0' = b_2 d_1 = b_2(1 - i)$$

where b_1 and b_2 are the start- and end-point derivative coefficients, respectively. In order to investigate the effect of the start derivative coefficient, the magnitude of the end-point derivative is kept constant, i.e., b_2=1, while the start-point derivative coefficient varies from 0.2 to 3 with an increment of 0.2. The resulting curves are shown in Fig. 2a. The original P-H curve is also depicted with b_1=b_2=1. It has been observed that increasing the magnitude of the start-point derivative results in stretching the curve along the start-point derivative vector and increasing the curvature of the curve at the returning point. By contrast, decreasing the b_1 coefficient causes the curve to turn sooner and decreases the curvature at the returning point. Similarly, for investigating the effect of the end-derivative coefficient, the magnitude of the start-point derivative is kept constant, i.e., b_1=1, while the end-point derivative coefficient varies from 0.2 to 3. The resulting curves are shown in Fig. 2b.

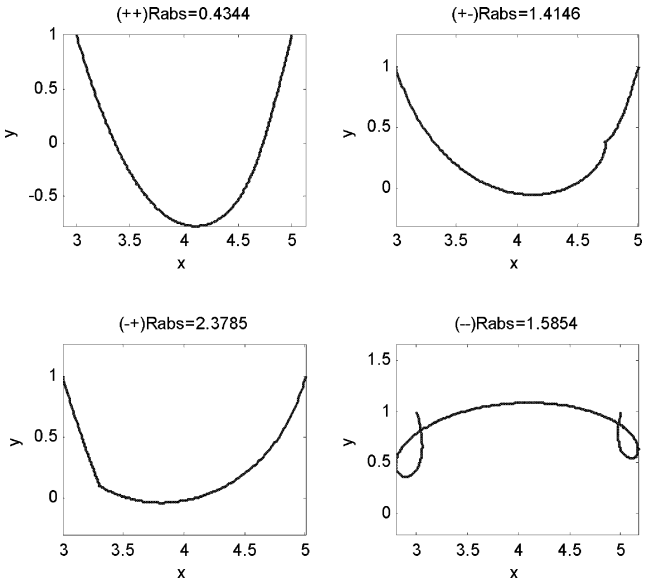

Fig. 1 The four Pythagorean hodograph (P-H) quintic interpolants with $r_0 = 3 + i$, $r_1 = 5 + i$, $d_0 = 3 - 10i$ and $d_1 = 2 + 8i$

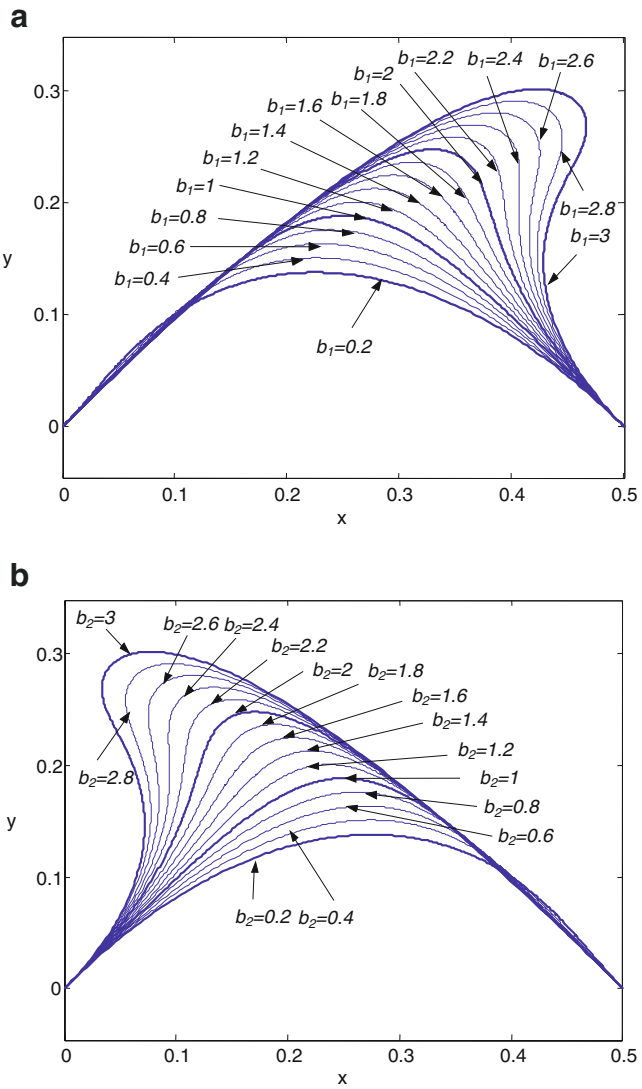

Fig. 2 Effect of b_1 and b_2 coefficients on the P-H shape. **a** Effect of b_1 variation (b_2=1). **b** Effect of b_2 variation (b_1=1)

3 Real-time interpolation by P-H quintic curves

Real-time interpolation by P-H quintic curves was proposed by Farouki and Sagar [10] in 1995. They

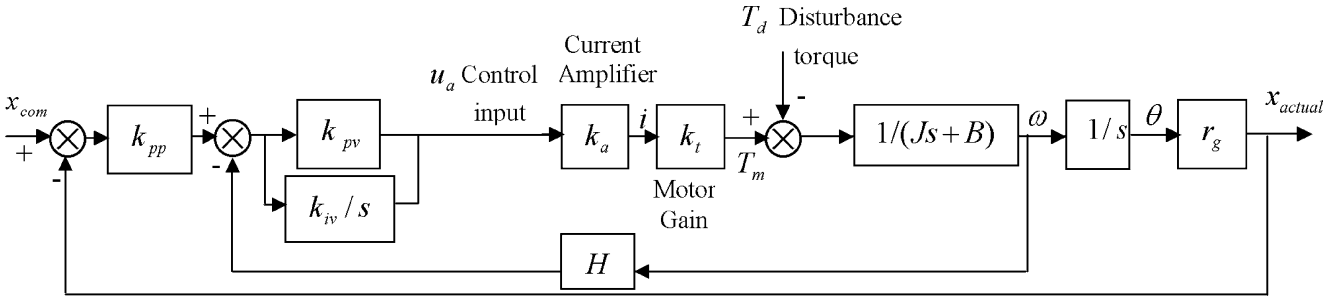

Fig. 3 Block diagram of the P-PI servo controller

presented formulations and analyses where the feed rate on the P-H curve is specified as a constant, linear, or quadratic function of the arc length. For constant feed rate, the arc length value is:

$$s(\xi_k) = k\Delta s_0 \tag{8}$$

where $\Delta s_0 = v_0 \Delta t$ is the arc length in iteration k, Δt is the sampling period, and v_0 is the feed rate. The desired sequence of parameter values $\xi_1, \xi_2, \ldots, \xi_N$ is computed by Eq. 8. This equation has a unique real root ξ_k, which can be determined using the Newton-Raphson method as follows:

$$\xi_k^{(r)} = \xi_k^{(r-1)} - \frac{s\xi_k^{(r-1)} - k\Delta s_0}{\sigma\left(\xi_k^{(r-1)}\right)}, \quad r = 1, 2, \ldots \tag{9}$$

An initial approximation for each iteration can be computed from the following equation [10]:

$$\xi_k^0 = \xi_{k-1} + \frac{\Delta s_0}{\sigma(\xi_{k-1})} \tag{10}$$

4 Dynamic model of the feed drive

The linear dynamic model of a P-PI servo controller defined for classical feed drives is shown in Fig. 3. This controller is a commonly used structure in CNC drive systems [6]. The control signal u_a [v] is applied to the current amplifier, which has a gain of k_a [A/v]. The motor torque T_m [N.m] is obtained by multiplication of the motor current i [A] and the motor gain k_t [N.m/A]. The positional loop is closed by the P controller, which has a proportional gain k_{pp} [v/mm] and the velocity loop is closed by the PI controller, which has a proportional gain of k_{pv} [v/v] and an integral gain of k_{iv} [v/v]. The total torque delivered by the motor should overcome the external disturbance torque, the inertial load, and the system's viscous damping, which are identified by T_d [N.m], J [kg.m^2], and B [kg.m^2/s], respectively [14]. After computing the angular velocity ω [rad/s], the angular position of the motor shaft θ [rad] is obtained by integration. The linear displacement of the table is then computed using the transmission ratio, r_g [mm/rad]. The feedback control law in Laplace domain is written as follows:

$$u_a(s) = \left[(x_{com} - x_{act})k_{pp} - H\omega(s)\right]\left(k_{pv} + \frac{k_{iv}}{s}\right) \tag{11}$$

where H [v.s/rad] is the velocity feedback gain, and the angular velocity and the actual position are expressed as:

$$\omega(s) = \frac{k_t k_a}{Js + B} u_a(s) \tag{12}$$
$$x_{act}(s) = \frac{r_g}{s}\omega(s) = \frac{r_g}{s} \cdot \frac{k_t k_a}{Js + B} u_a(s)$$

The feed drive and the controller parameters are summarized in Table 1 [15].

5 The over-corner P-H curve approach

A large phase lag is generated when a low bandwidth servo controller, such as a P-PI servo controller, is used. Thus, the actual tool path before reaching the sharp

Table 1 Axis feed drive and controllers parameters

Feed drive parameters		X-axis	Y-axis
Current amplifier gain, k_a (A/v)		6.4898	7.5768
Motor gain, k_t (N.m/A)		0.4769	0.4769
Total reflected inertia, J (kg.m^2)		0.0077736	0.009811
Viscous damping, B (kg.m^2/s)		0.019811	0.028438
Transmission gain, r_g (mm/rad)		1.5915	1.5915
PI controller parameters for the velocity loop:			
Velocity feedback gain, H (v.s/rad)		1	1
Proportional gain, k_{pv} (v/v)		1	1
Integral gain, k_{iv} (v/v)		0.5	0.5
P controller parameters for the position loop:			
Proportional gain, k_{pp} (v/mm)	For α=90°	19.2	19.2
	For α=60°	20.1	20.1
	For α=30°	20.53	20.53

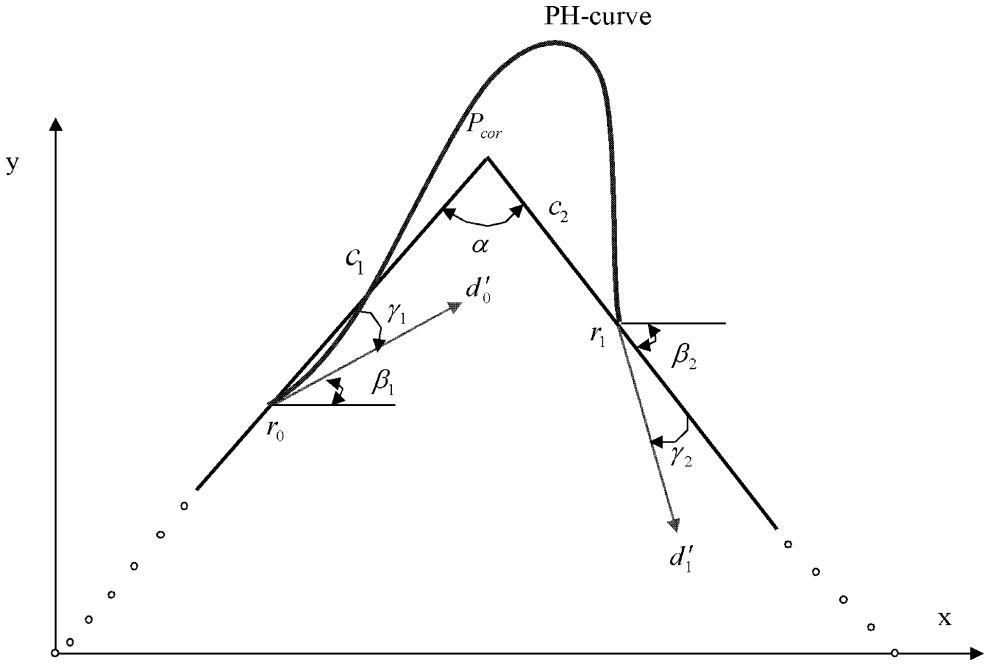

Fig. 4 Geometry of a corner and the modified P-H tool path

corner turns and follows the other linear segment of the corner, which results in an undesired undercut and a significant cornering error.

The over-corner P-H approach is based on the following idea. One P-H curve is constructed over the corner region. The position commands are generated using the newly constructed P-H curve, thus, the actual tool path gets closer to the linear segments of the corner and maintain the cornering error within a certain limit. Using this approach, the tool turns around the sharp corner without stopping. The geometry of the modified tool path for the over-corner P-H approach is introduced in Fig. 4. c_1 and c_2 are the distances of the start- and end-points of the P-H curve from the corner tip, P_{cor}. The values of c_1 and c_2 depend on Δ_{max}, which is the maximum value of the cornering error. The position of the start- and end-points of the P-H curve are:

$$\begin{aligned} r_0 &= (L - c_1)\sin\ \alpha/2\ + (L - c_1)\cos(\alpha/2)i \\ r_1 &= (L + c_2)\sin\ \alpha/2\ + (L - c_2)\cos(\alpha/2)i \end{aligned} \tag{13}$$

where L is the length of the corner edge and α is the corner angle. Also, the start and end derivatives are:

$$\begin{aligned} d_0 &= 1 + \tan(\beta_1)i, \\ d_1 &= 1 - \tan(\beta_2)i \end{aligned} \tag{14}$$

where β_1 and β_2 are:

$$\begin{aligned} \beta_1 &= \pi/2 - \alpha/2 - \gamma_1 \\ \beta_2 &= \pi/2 - \alpha/2 + \gamma_2 \end{aligned} \tag{15}$$

In the above relations, γ_1 and γ_2 are the correction angles for the start- and end-points of the P-H curve, respectively. The corrected end-derivatives are:

$$\begin{aligned} d_0' &= b_1[1 + \tan(\pi/2 - \alpha/2 - \gamma_1)i] \\ d_1' &= b_2[1 + \tan(\pi/2 - \alpha/2 + \gamma_2)i] \end{aligned} \tag{16}$$

where b_1 and b_2 are the end-derivative magnitude coefficients. The correction parameters γ_1, b_1, γ_2, and b_2 for the P-H curve have a large influence on the actual tool path, which is generated by real-time simulation. These parameters can be selected for maintaining the cornering error within a certain limit.

6 Simulations

The original tool path consists of two 50-mm linear segments. A constant feed rate of 100 mm/s is used for

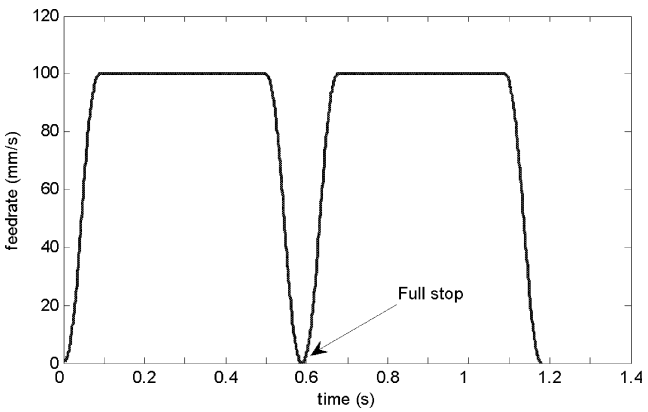

Fig. 5 Original feed rate profile for the corner α=90°

Table 2 Geometric parameters of the constructed P-H curves

P-H parameters	α=90°	α=60°	α=30°
b_1	1.69	0.975	0.38
b_2	1.15	0.77	0.35
γ_1	−3.25°	−2°	0°
γ_2	0°	2°	1°

traveling along linear segments. To achieve an S-shaped feed rate profile, a jerk-limited approach with a maximum jerk of 50,000 mm/s^3 and a maximum acceleration of 2,000 mm/s^2 is used [16]. The original feed rate profile for the case of α=90° is shown in Fig. 5. As can be seen, each linear segment has three parts: acceleration from full stop, constant feed rate, and deceleration to full stop. The geometric parameters of the constructed P-H curves over

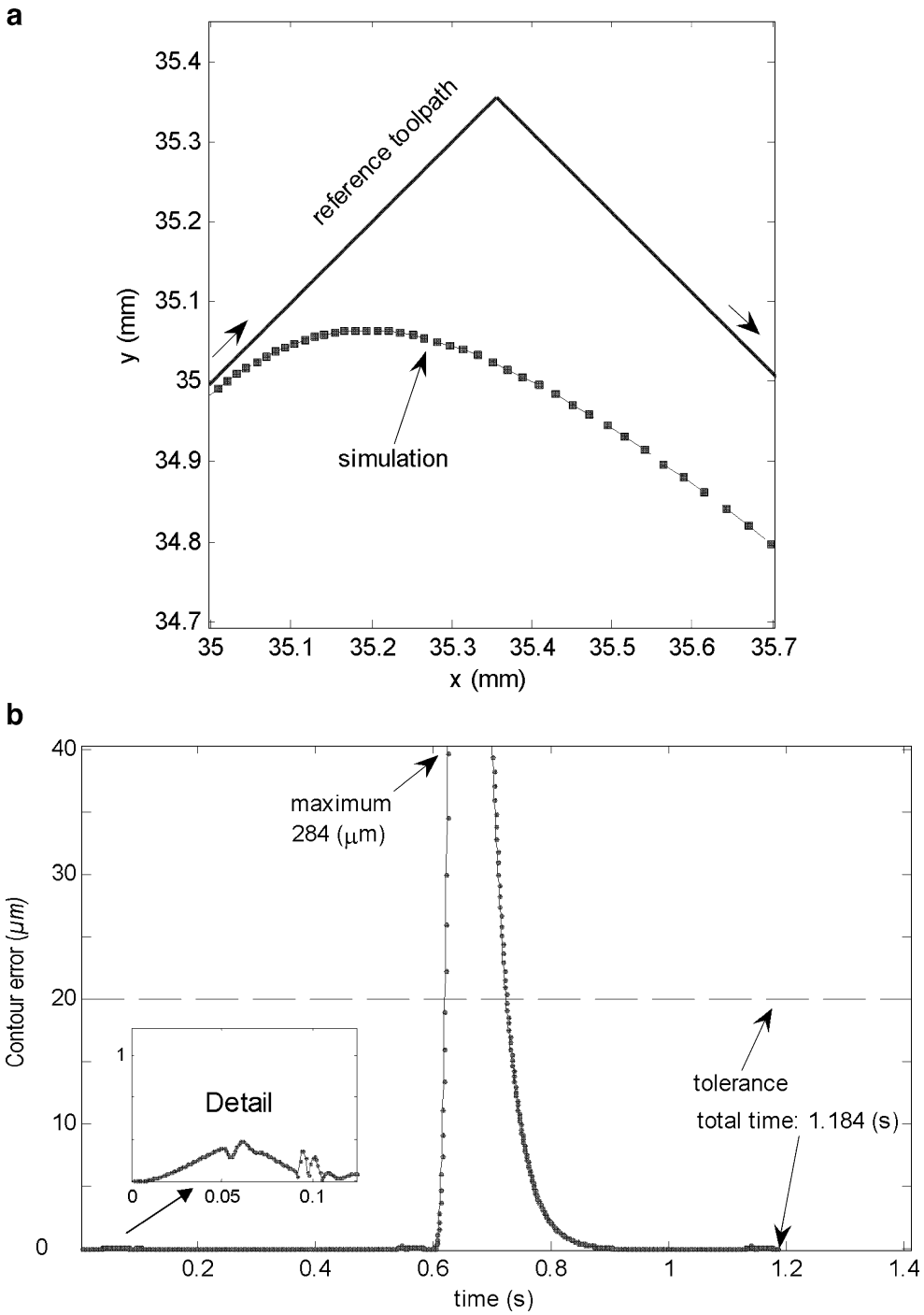

Fig. 6 Original tool path performance for α=90° with the P-PI servo controller. **a** Cornering performance. **b** Cornering error profile

the corner with angles of 90°, 60°, and 30° are presented in Table 2. The values of γ_1 and γ_2 are obtained by comparing the results of numerical simulation and choosing the best values which minimize the cornering error. In all cases, c_1 and c_2 are equal to 0.18 mm and Δt is equal to 1 ms.

Simulation results for the 90° angle are shown in Figs. 6 and 7. In Fig. 6a, it can be observed that the P-PI controller is not able to turn the sharp corner correctly and that there is a large cornering error. The maximum cornering error is 284 μm, which is shown in Fig. 6b. The modified tool path with the P-H curve is shown in Fig. 7a. The inset shows the real-time interpolation commands with a feed rate of 3.74 mm/s around the corner. The actual tool path is also depicted. The deviation error of the actual tool path from

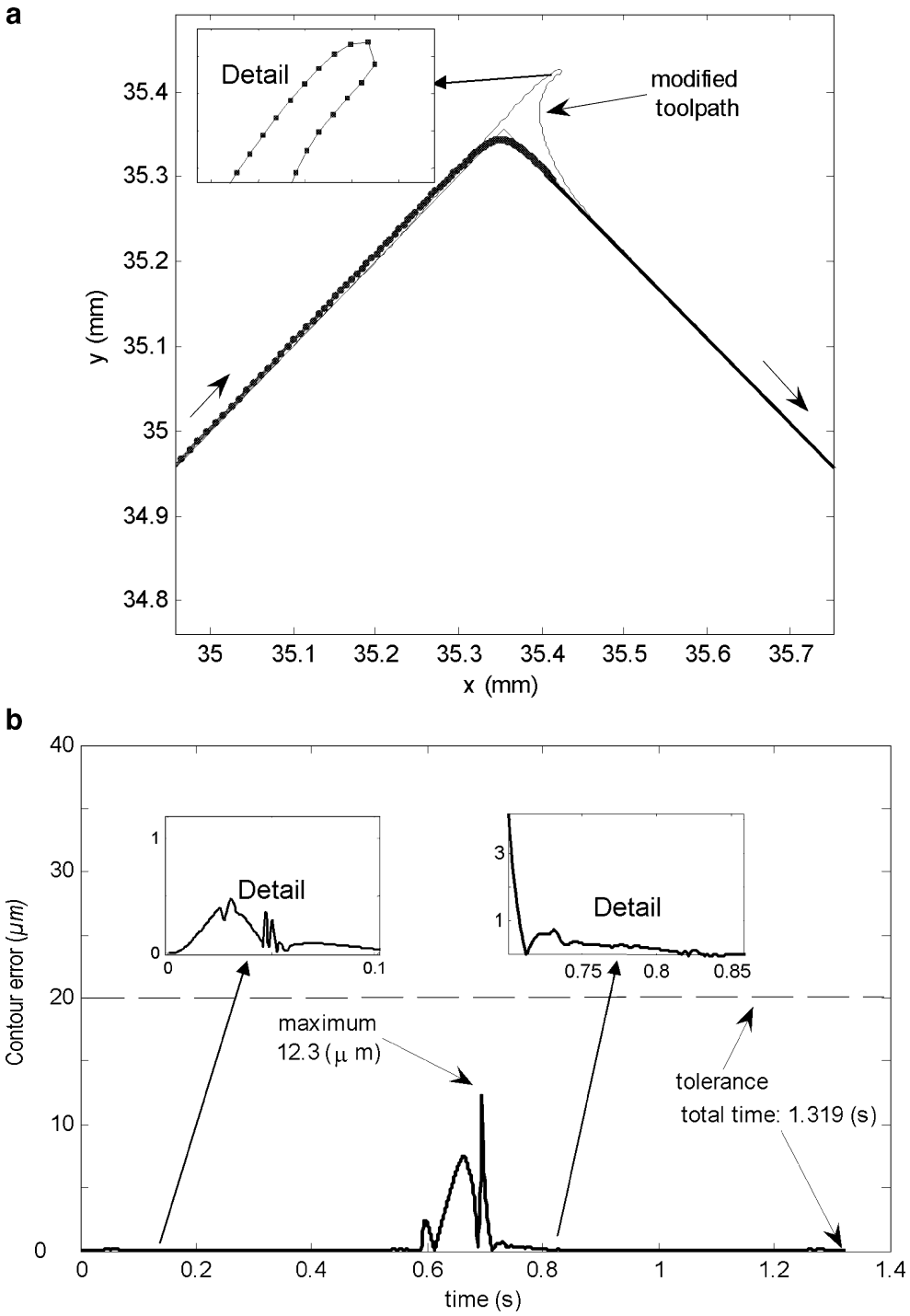

Fig. 7 Modified tool path performance for α=90° over-corner P-H curve with the P-PI servo controller. **a** Cornering performance. **b** Cornering error profile

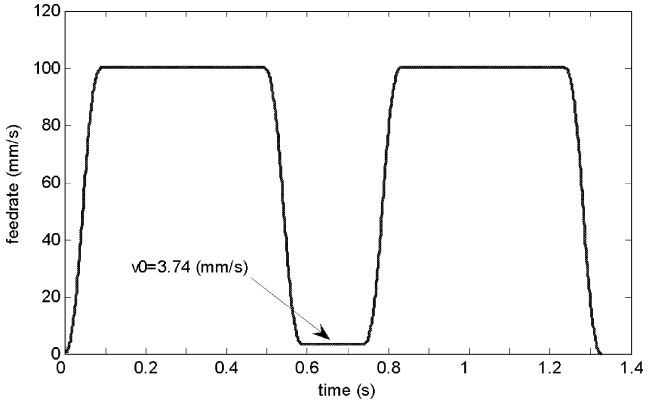

Fig. 8 Modified feed rate profile for the corner α=90°

the original tool path is shown in Fig. 7b. It can be observed that the maximum cornering error is 12.3 μm. The feed rate profile is shown in Fig. 8. The middle region feed rate is set to 3.74 mm/s for the P-H curve segment. The corner machining time is increased by small amount by 11.4% with respect to the original tool path. However, the amount of maximum cornering error is reduced to the allowable tolerance limit, which is 20 μm. According to Table 2, the geometric parameters of the P-H curve for this case (α=90°) are as follows: b_1=1.69, b_2=1.15, γ_1=−3.25°, and γ_2=0°. The magnitude of the start-point derivative is greater than the magnitude of the end-point derivative, which results in more stretching of the curve

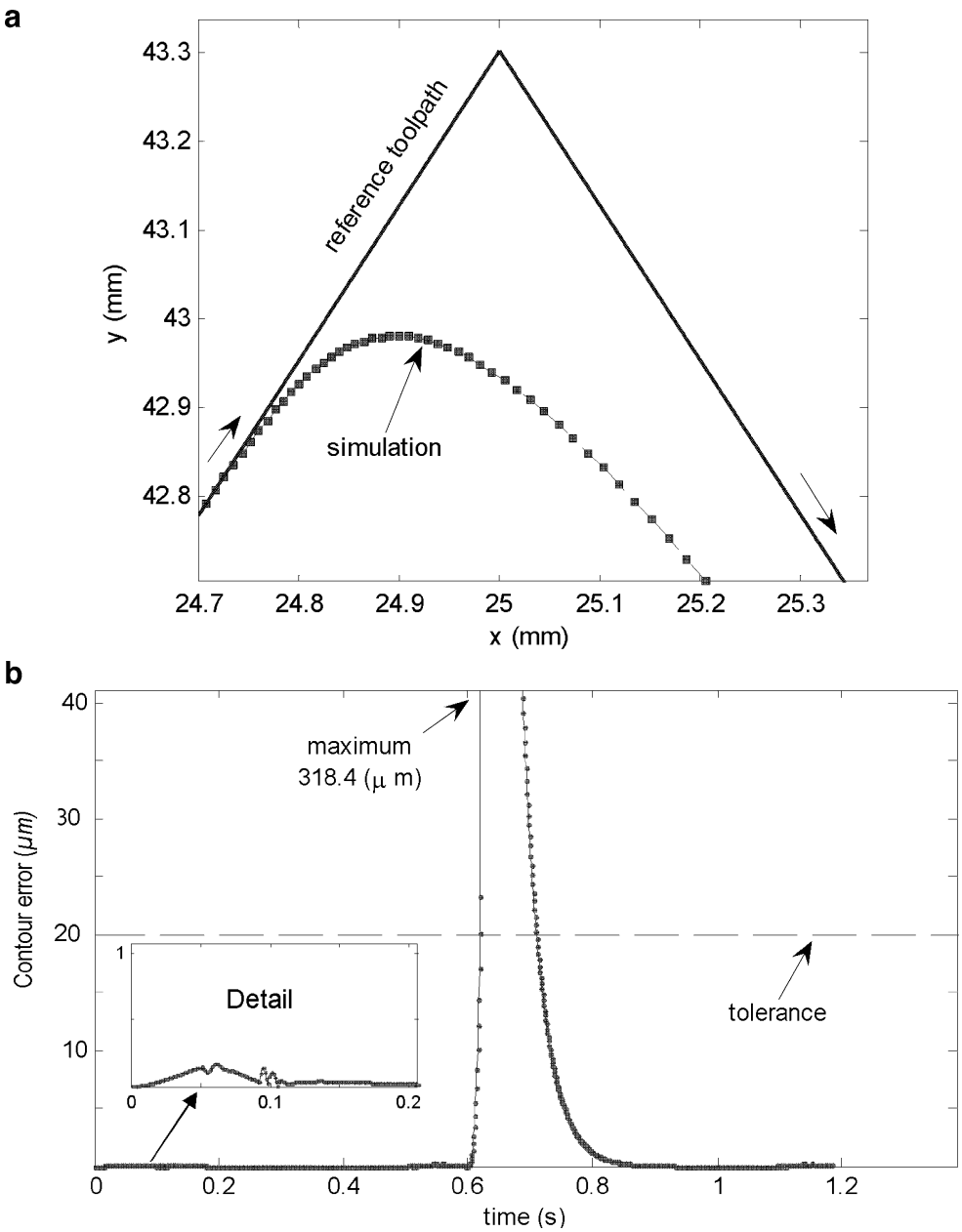

Fig. 9 Original tool path performance for α=60° with the P-PI servo controller. **a** Cornering performance. **b** Cornering error profile

along the first linear segment of the corner. The correction of the commands according to the stretched curve cause the actual tool path reach closer to the corner. Also, the tool path will follow the second linear segment of the corner more closely. In addition, γ_1 and γ_2 have a great influence on the amount of cornering error. If a small negative angle is chosen for γ_1, the actual tool path will follow the sharp corner closely and the cornering error will be reduced.

Simulation results for the 60° angle are shown in Figs. 9 and 10. There is a large cornering error equal to 318.4 μm, which is shown in Fig. 9b. The modified tool path with the P-H curve is shown in Fig. 10a. The inset shows the real-time interpolation commands with a feed rate of 3.72 mm/s around the corner. The actual tool path is also depicted. The deviation error of the actual tool path from the original tool path is shown in Fig. 10b.

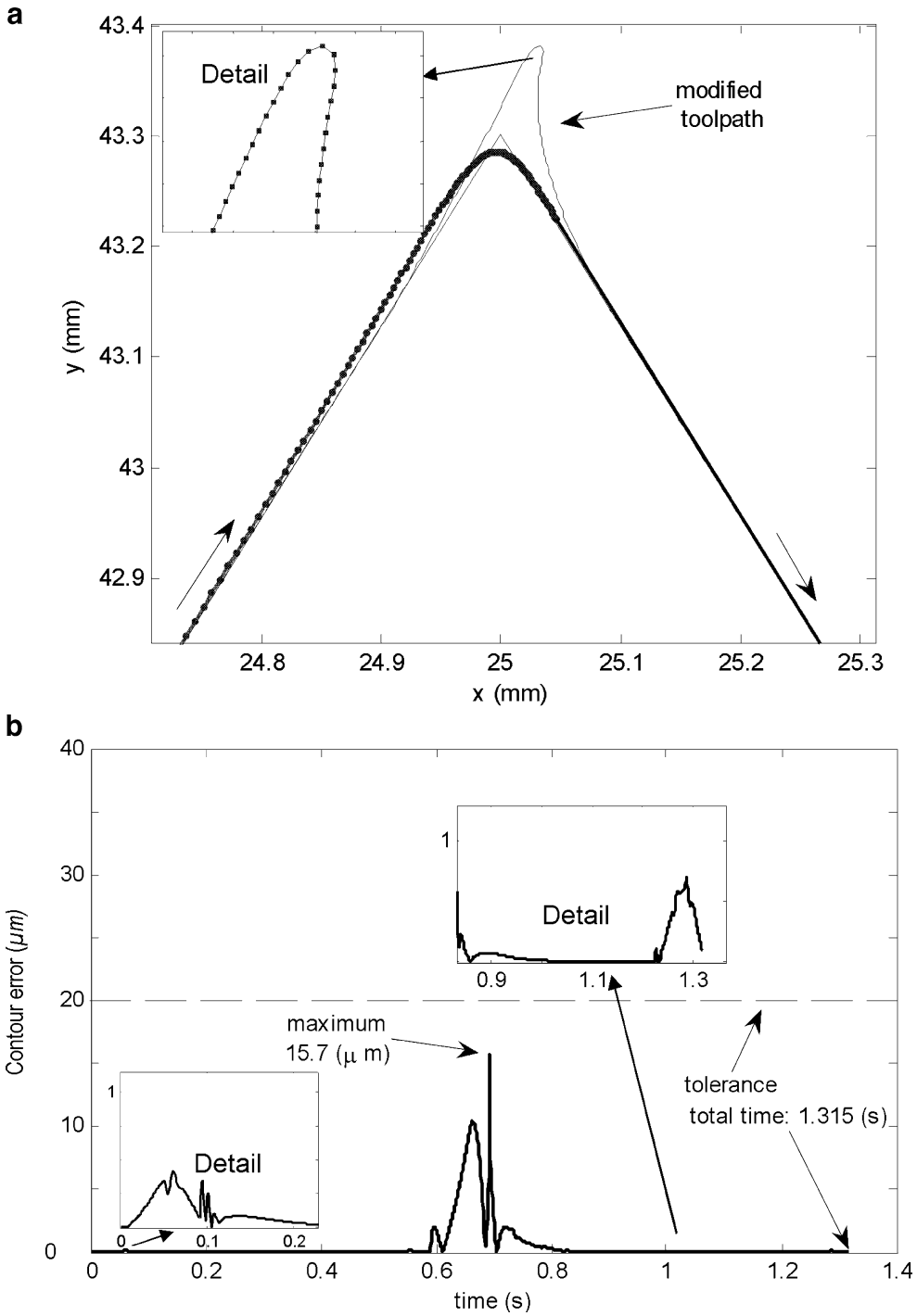

Fig. 10 Modified tool path performance for α=60° over-corner P-H curve with the P-PI servo controller. **a** Cornering performance. **b** Cornering error profile

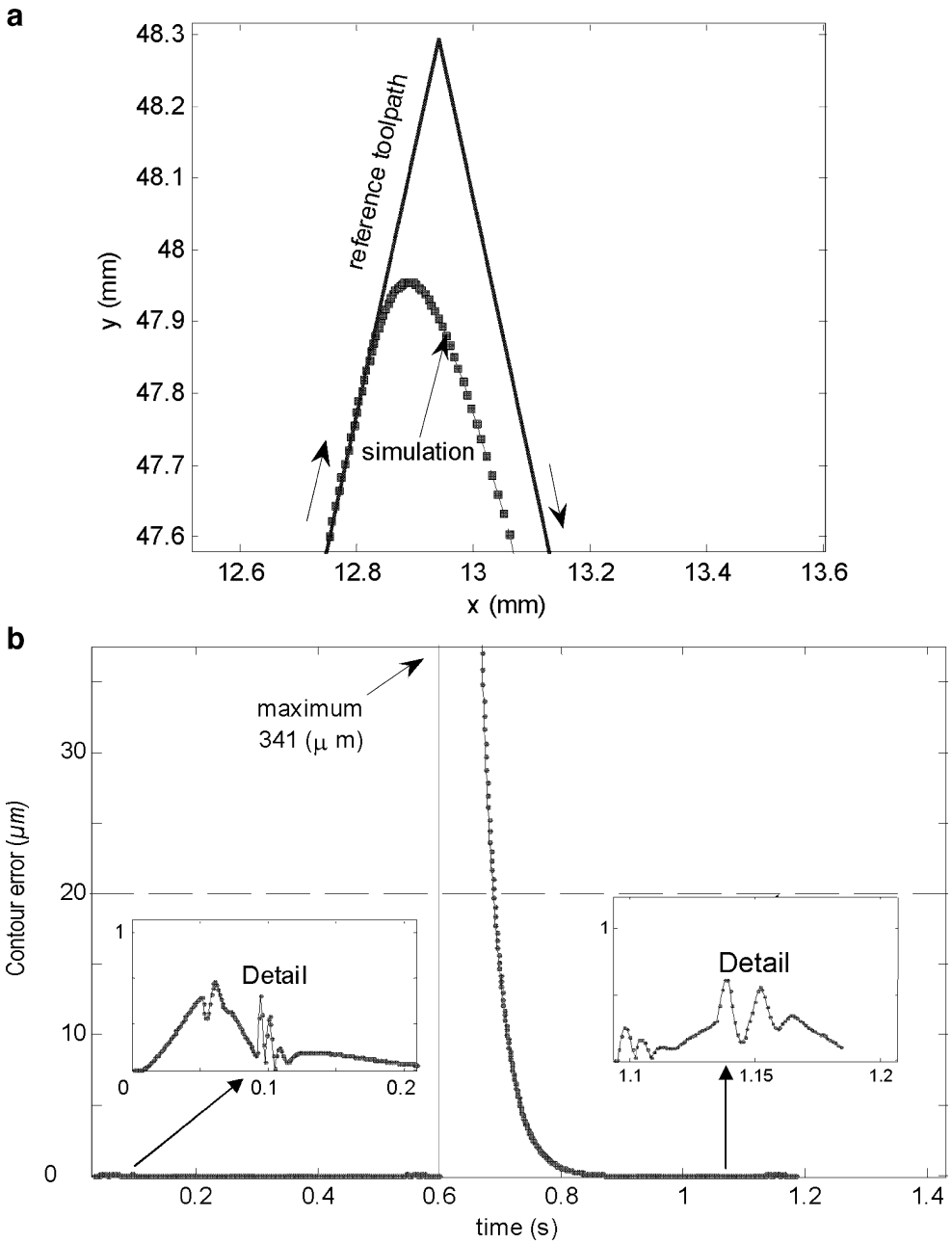

Fig. 11 Original tool path performance for α=30° with the P-PI servo controller. **a** Cornering performance. **b** Cornering error profile

It has been observed that the maximum cornering error is 15.7 μm. The corner machining time is increased to 1.315 s (for the modified tool path), which is 11% longer, but the amount of maximum cornering error is reduced to the allowable tolerance limit.

The results for the 30° angle are shown in Figs. 11 and 12, which carry a similar trend to those obtained for the 90° and 60°angles. In this case, the maximum cornering error is 341 μm for the sharp corner. By introducing the over-corner P-H curve which is traveled with the feed rate of 2.62 mm/s, the maximum value of cornering error is reduced to 16.5 μm. The corner machining time is increased to 1.357 s (for the modified tool path), which is 14.6% longer, but the amount of maximum cornering error is reduced to the allowable tolerance limit. Table 3 summarizes the results of the 90°, 60°, and 30°cases.

The geometric parameters of the P-H curve for the case of α=30° are: b_1=0.38, b_2=0.35, γ_1=0°, and γ_2=1°. The small positive correction angle γ_2 has a great effect on the amount of cornering error. For example, if γ_2=0° (the constructed P-H curve is tangential to the second linear segment of the corner at the end-point) is used while the other geometric

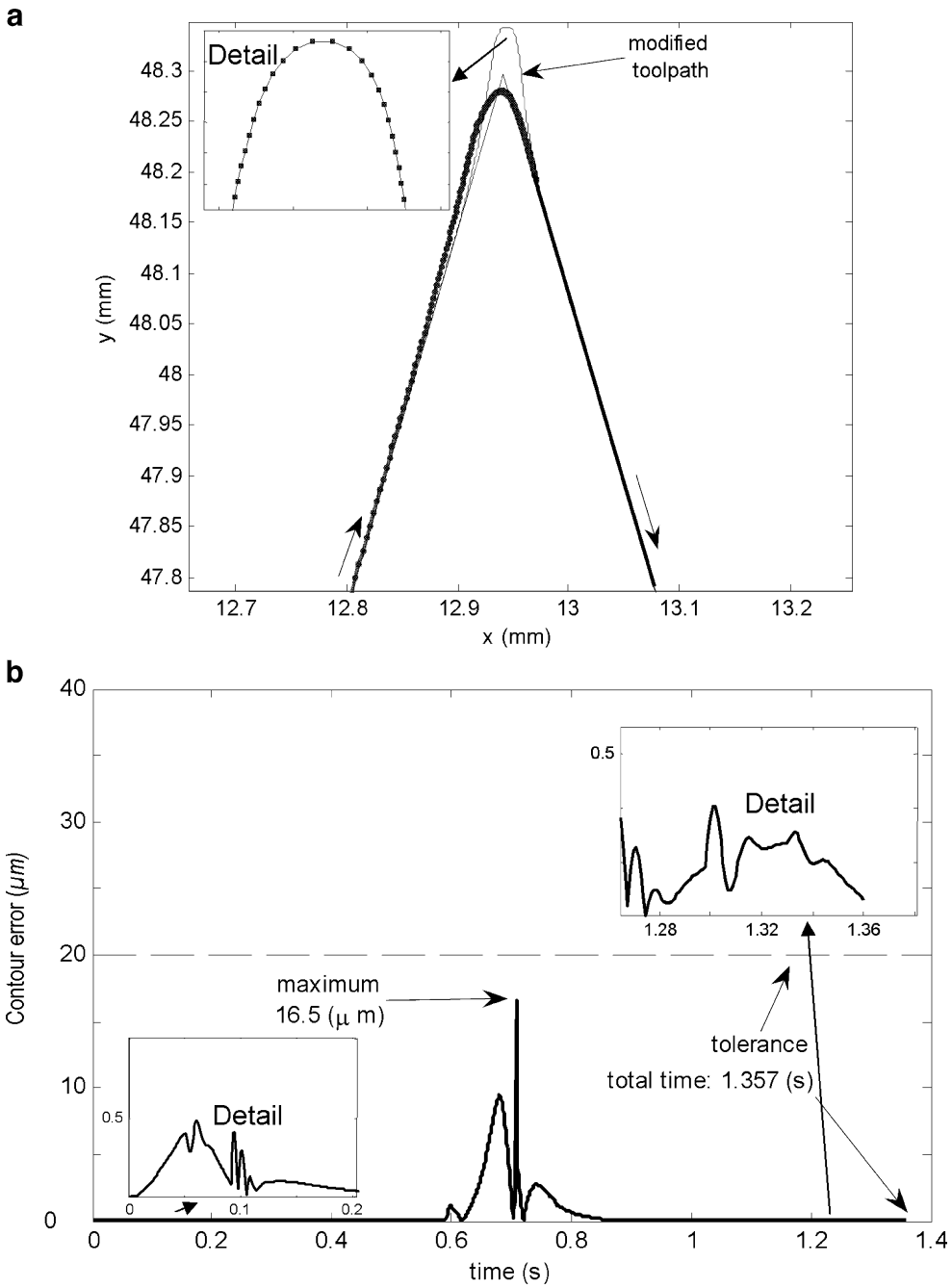

Fig. 12 Modified tool path performance for α=30° over-corner P-H curve with the P-PI servo controller. **a** Cornering performance. **b** Cornering error profile

Table 3 Summary of the cornering results, with an allowable tolerance limit of 20 μm

Corner tool path	Maximum cornering error (μm)	Relative corner machining time (%)
90°: sharp corner	284	100
90°: P-H curved corner	12.3	111.4
60°: sharp corner	318.4	100
60°: P-H curved corner	15.7	111
30°: harp corner	341	100
30°: P-H curved corner	16.5	114.6

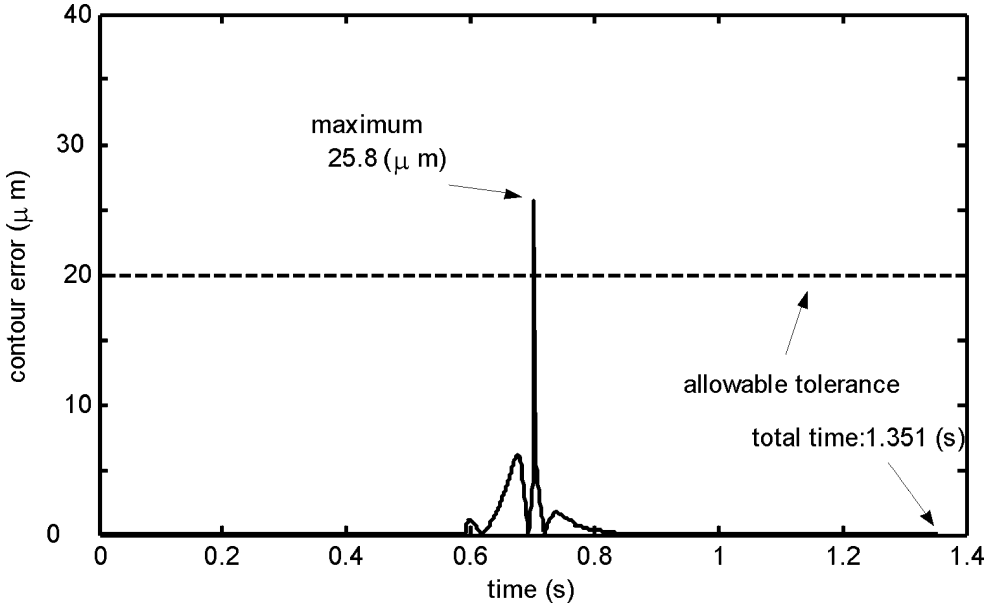

Fig. 13 Cornering error profile for the case $\alpha=30°$ and $\gamma_2=0°$

parameters of the P-H curve and the feed rate are kept constant, the amount of cornering error exceeds the allowable tolerance limit, which is 20 μm (see Fig. 13). But if $\gamma_2=1°$ is chosen, the amount of cornering error reaches 16.5 μm, (see Fig. 12b).

In this paper, the feed drives specification, jerk-limited parameters, and the feed rate on the original tool path are chosen according to [6, 15]. The simulation results of the proposed method shows that the amount of cornering error is improved by about 30% compared with the results obtained by Erkorkmaz et al. [6]. In addition, the total machining time is also decreased by an amount between 3% and 6%.

7 Conclusions

The method presented for corner machining is based on Pythagorean hodograph (P-H) curve theory. Compared with the previously proposed methods, such as circular arc, double clothoid, and three-segment quintic spline methods, the newly developed over-corner P-H curve approach holds superior flexibility. The geometric parameters of the P-H curve, such as end-derivatives and their magnitude, can be chosen according to the corner angle in order to keep the tracking deviations within the specified tolerance limit. In addition, the real-time interpolation of the P-H curve, which is defined for the modified tool path, is computed accurately and efficiently by the Newton-Raphson method. The proposed approach introduces one arc-length parametric P-H curve for the whole corner, thus, there is no feed rate fluctuation along the actual tool path. The simulation results for 30°, 60°, and 90° corners confirm that the over-corner P-H approach is capable of decreasing the corner error and maintaining the tracking accuracy within a certain limit.

References

1. Altintas Y, Erkorkmaz K (2003) Feedrate optimization for spline interpolation in high speed machine tools. Annals CIRP 52 (1):297–302
2. Jouaneh MK, Wang Z, Dornfeld DA (1988) Tracking of sharp corners using a robot and a table manipulator. In: Proceeding of the USA-Japan Symposium on Flexible Automation, Minneapolis, Minnesota, July 1988, pp 271–278
3. Jouaneh MK, Wang Z, Dornfeld DA (1990) Trajectory planning for coordinated motion of a robot and a positioning table. Part 1. Path specification. IEEE Trans Robot Automat 6(6):735–745
4. Jouaneh MK, Wang Z, Dornfeld DA (1990) Trajectory planning for coordinated motion of a robot and a positioning table. Part 2. Optimal trajectory specification. IEEE Trans Robot Automat 6 (6):746–759
5. Kanayama Y, Miyake N (1986) Trajectory generation for mobile robots. In: Proceedings of the 3rd International Symposium on Robotics Research, Paris, France, October 1985, pp 337–340
6. Erkorkmaz K, Yeung C-H, Altintas Y (2006) Virtual CNC System. Part II. High speed contouring application. Int J Mach Tool Manufact 46(10):1124–1138
7. Moon HP, Farouki RT, Choi HI (2001) Construction and shape analysis of PH quintic Hermite interpolants. Comput Aided Geom Des 18(2):93–115
8. Farouki RT, Tsai YF (2001) Exact Taylor series coefficients for variable-feedrate CNC curve interpolators. Comput Aided Geom Des 33(2):155–165
9. Farouki RT, Sakkalis T (1990) Pythagorean Hodographs. IBM J Res Dev 34(5):736–752
10. Farouki RT, Sagar Shah (1995) Real-time CNC interpolators for Pythagorean-hodograph curves. Comput Aided Geom Des 13 (7):583–600
11. Erkorkmaz K, Altintas Y (2005) Quintic spline interpolation with minimal feed fluctuation. J Manuf Sci Eng—Trans ASME 127 (2):339–349
12. Farouki RT, Manjunathaiah J, Yuan GF (1997) G codes for the specification of Pythagorean-hodograph tool paths and associated feedrate functions on open-architecture CNC machines. Int J Mach Tool Manufact 39(1):123–142
13. Erkorkmaz K, Altintas Y (1998) High speed contouring control algorithm for CNC machine tools. In: Proceedings of the ASME

International Mechanical Engineering Congress and Exposition (IMECE'98), Anaheim, California, November 1998, Dynamic Systems and Control division (DSC), vol 64, pp 463–469
14. Erkorkmaz K, Altintas Y (2001) High speed CNC system design. Part II: modeling and identification of feed drives. Int J Mach Tool Manufact 41(10):1478–1509
15. Yeung CH, Altintas Y, Erkorkmaz K (2006) Virtual CNC System. Part I. System architecture. Int J Mach Tool Manufact 46 (10):1107–1123
16. Erkorkmaz K, Altintas Y (2001) High speed CNC system design. Part I: jerk limited trajectory generation and quintic spline interpolation. Int J Mach Tool Manufact 41(9):1323–1345